Journal of ELECTRONIC MATERIALS, Vol. 45, No. 9, 2016
DOI: 10.1007/s11664-016-4566-6

High-Operating Temperature HgCdTe: A Vision for the Near Future

D. LEE,[1,3] M. CARMODY,[1] E. PIQUETTE,[1] P. DREISKE,[1] A. CHEN,[1] A. YULIUS,[1] D. EDWALL,[1] S. BHARGAVA,[1] M. ZANDIAN,[1] and W.E. TENNANT[2]

1.—Teledyne Imaging Sensors, 5212 Verdugo Way, Camarillo, CA 93012, USA. 2.—Tennant Electro Optics Consulting Inc., 1579 Calle Yucca, Thousand Oaks, CA 91360, USA. 3.—e-mail: donald.lee@teledyne.com

We review recent advances in the HgCdTe material quality and detector performance achieved at Teledyne using molecular beam epitaxy growth and the double-layer planar hetero-junction (DLPH) detector architecture. By using an un-doped, fully depleted absorber, Teledyne's DLPH architecture can be extended for use in high operating temperatures and other applications. We assess the potential achievable performance for long wavelength infrared (LWIR) hetero-junction *p*-lightly-doped *n* or *p*-intrinsic-*n* (p-i-n) detectors based on recently reported results for 10.7 μm cutoff 1 K $\times$ 1 K focal plane arrays (FPAs) tested at temperatures down to 30 K. Variable temperature dark current measurements show that any Shockley–Read–Hall currents in the depletion region of these devices have lifetimes that are reproducibly greater than 100 ms. Under the assumption of comparable lifetimes at higher temperatures, it is predicted that fully-depleted background radiation-limited performance can be expected for 10-μm cutoff detectors from room temperature to well below liquid nitrogen temperatures, with room-temperature dark current nearly 400 times lower than predicted by Rule 07. The hetero-junction p-i-n diode is shown to have numerous other significant potential advantages including minimal or no passivation requirements for pBn-like processing, low 1/*f* noise, compatibility with small pixel pitch while maintaining high modulation transfer function, low crosstalk and good quantum efficiency. By appropriate design of the FPA dewar shielding, analysis shows that dark current can theoretically be further reduced below the thermal equilibrium radiative limit. Modeling shows that background radiation-limited LWIR HgCdTe operating with *f*/1 optics has the potential to operate within $\sqrt{2}$ of background-limited performance at 215 K. By reducing the background radiation by 2/3 using novel shielding methods, operation with a single-stage thermo-electric-cooler may be possible. If the background radiation can be reduced by 90%, then room-temperature operation is possible.

Key words: HgCdTe, hot detectors, LWIR, radiative-limit, auger-suppressed, p-i-n detector

INTRODUCTION

Within the last decade, significant effort has focused on the development of alternate detector technologies to HgCdTe including quantum well infrared photo detectors (QWIPS), strained-layer superlattice (SLS) and InAsSb, all based on III–V materials. These developments have two primary motivations: (1) the perceived challenges of reproducibly fabricating high-operability HgCdTe FPAs at reasonable cost and (2) theoretical predictions of

(Received January 20, 2016; accepted April 21, 2016; published online May 9, 2016)

lower Auger recombination for SLS detectors compared to HgCdTe. The predicted lower Auger recombination has been assumed to translate into a fundamental advantage for SLS over HgCdTe in terms of lower dark current and/or higher operating temperature.[1]

Despite the promise of the III–V based detectors, HgCdTe remains the highest-performing infrared (IR) material technology for a number of applications including low-background military and commercial space, airborne very long wavelength infrared (VLWIR) hyperspectral and astronomy. The superior performance is in part due to the fact that Auger recombination rate alone is not adequate to characterize the performance of a diffusion-limited detector. Additionally, the Auger-limited detector dark current is proportional to the absorber doping level, which for P-on-n HgCdTe can be made quite low. Furthermore, recent advances in HgCdTe promise to dramatically "move the goal posts" with the use of p-i-n hetero-junction detectors, leading to performance limited by radiative rather than Auger recombination, with a significant reduction in dark current. By suitably managing the detector shielding, the radiative background can be further suppressed for additional potential reduction in dark current and/or increase in operating temperature.

Although the appeal of higher-performance HgCdTe for applications with demanding requirements is obvious, there are also many situations where integrated Dewar-cooler assembly (IDCA) or camera cost is paramount. These costs are often assumed to be driven primarily by the size and cost of the substrate. Although cadmium zinc telluride (CZT) substrates are substantially more expensive than those used for III–V detectors, the drive towards smaller pixel pitch has a proportionately greater impact in reducing the per die fabrication cost for HgCdTe relative to other substrate-independent costs such as the Dewar and cooler. By operating HgCdTe at radiative or sub-radiative background limits, it may be possible to operate at sufficiently high operating temperatures whereby cryo-cooling or thermo-electric cooling is no longer required, providing for a reduction in Dewar/cooler size, weight and power (SWaP) as well as overall product cost. Additionally, CZT substrate size as well as MBE reactor capacity are increasing, with 7 cm × 7 cm substrates now in production at Teledyne and the first 8 cm × 8 cm growths (equivalent to 5 inch diameter), now demonstrated, as shown in Fig. 1. The impact of substrate cost is further reduced by the drive toward smaller pixel pitch, pixel over-sampling and faster optics which decrease optics size and cost.

The drive towards smaller pixel pitch is also advantageous in enhancing the operability of HgCdTe detectors. FPA inoperability is fundamentally related to the dislocation density of the substrate and scales with pixel area; hence, as the pixel size is reduced, the operability of the FPA increases. As we shall show, for many cases, the operability that can be achieved with the present levels of obtainable defects is more than adequate for many applications.

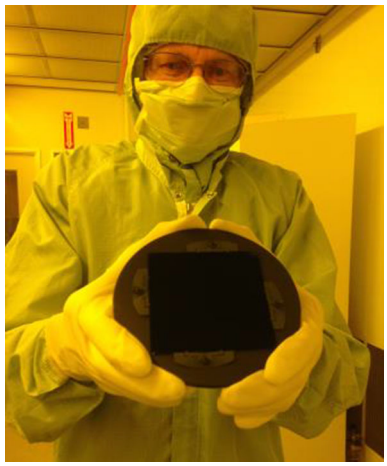

Fig. 1. 8 cm × 8 cm HgCdTe wafer grown by MBE at Teledyne.

THE ROLE OF AUGER LIFETIME IN DETECTOR PERFORMANCE

An ideal P-on-n detector limited by Auger-1 recombination has a current density, J^{A}, described by the relationship

$$J^{\mathrm{A}} = q\frac{n_{\mathrm{i}}^2}{n\tau_{\mathrm{A}}}d, \tag{1}$$

where q is the unit of electrical charge, n is the electron concentration, d is the absorber thickness, n_{i} is the intrinsic carrier concentration and τ_{A} is the Auger-1 lifetime. The Auger-1 lifetime in n-type material is related to the hole, electron and intrinsic carrier concentrations and the intrinsic Auger-1 lifetime, τ_{Ai}, by[2]

$$\tau_{\mathrm{A}} = \frac{2\tau_{\mathrm{Ai}}n_{\mathrm{i}}^2}{n(n+p)}, \tag{2}$$

where p is the hole concentration. By inserting the expression for the Auger lifetime into Eq. 1, the current density can be evaluated in two limits. For the intrinsic or high operating temperature limit, where $p \cong n = n_{\mathrm{i}}$, we obtain

$$J^{\mathrm{A}} \cong q\frac{n_{\mathrm{i}}}{\tau_{\mathrm{Ai}}}d. \tag{3}$$

For the extrinsic or low operating temperature limit, where $p \ll n \cong N_{\mathrm{d}}$, where N_{d} is the absorber doping level, we have

$$J^{\mathrm{A}} \cong \frac{qN_{\mathrm{d}}d}{2\tau_{\mathrm{Ai}}}. \tag{4}$$

For both cases, the Auger-limited current density is observed to be inversely proportional to the intrinsic Auger-1 lifetime, τ_{Ai}. The larger predicted Auger lifetime for SLS detectors compared to HgCdTe is one of the key reasons for interest in this material technology. Note, however, in the extrinsic operating regime, the dark current density is also proportional to the doping density, which can be made very low for HgCdTe.

In the intrinsic regime, the current density is independent of doping and dominated by the intrinsic carrier concentration. For an Auger-limited detector, a larger intrinsic Auger-1 lifetime permits operation at somewhat higher temperatures; however, the impact is relatively minor compared to the exponential increase in dark current with increasing temperature.

AUGER-SUPPRESSED DETECTOR PERFORMANCE

Auger suppression provides a method to reduce detector dark current, and is particularly effective in the intrinsic (HOT) operating range and has been widely described in the literature.[3–5] Figure 2a shows a schematic for a P-on-n detector at zero bias and operating in the intrinsic regime. Here, capital letters indicate a wider bandgap and lower case letters indicate the active (narrowest) bandgap layer. The number of holes and electrons in the absorber region are equal to n_i. Under reverse bias, holes diffuse to the junction and are removed by the p-contact. If the removal rate is greater than the ability of the n-contact region to re-supply, then, in order to maintain charge neutrality, an equivalent number of electrons are removed from the n-contact and the residual n-carrier concentration is equal to the number of ionized donors. This situation is shown in Fig. 2b and is known as Auger-suppression.

With ideal Auger suppression, the electron concentration is equal to the donor concentration and the Auger lifetime is enhanced by the square of the ratio of the intrinsic to extrinsic carrier concentrations. Figure 3 shows the predicted ratio of Auger-suppressed to Auger-limited dark current for 10 μm cutoff wavelength P-on-n HgCdTe as a function of temperature and doping. As expected, Auger suppression has a significant impact in the intrinsic (HOT) temperature region due to the sweep-out of a large number ($n_i \gg N_d$) of intrinsic carriers. The impact is larger for lower levels of n-doping since the intrinsic carrier concentration is proportionately higher. Figure 4 shows the predicted dark current density for Auger-suppressed detectors as a function of temperature and doping for 10 μm cutoff wavelength P-on-n HgCdTe.

As predicted by Eq. 4, the dark current decreases linearly with doping until the background radiation-limit is reached. It should be noted that Rule 07, which is an empirical fit to the performance of Teledyne detectors doped at a nominal value of $1 \times 10^{15}/cm^3$, reflects the observed effects of Auger suppression for this doping.[6,7] Thus, in the intrinsic region, Rule 07 represents significantly better performance than the Auger limit. Figure 4 shows the range of low doping that can be reproducibly generated in Teledyne growths by MBE. At this

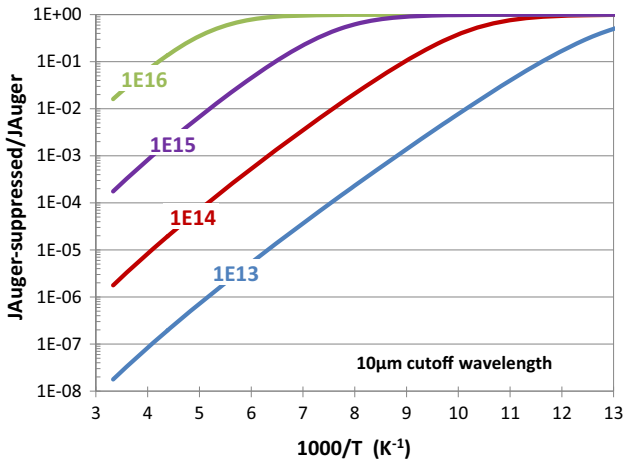

Fig. 3. Auger suppression dramatically decreases dark current at intrinsic temperatures.

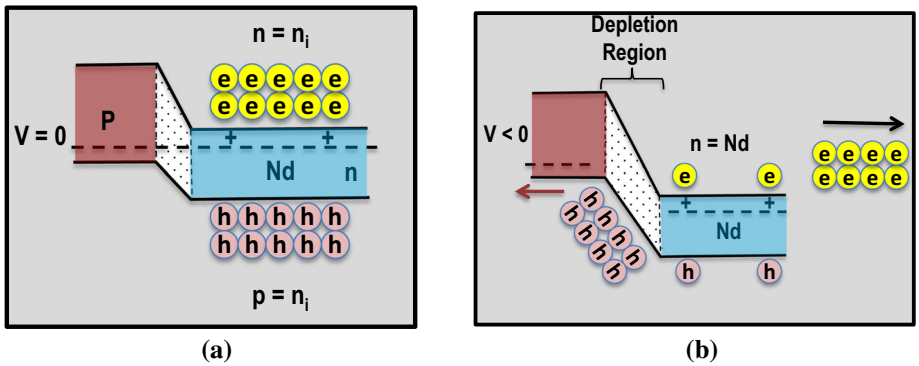

Fig. 2. (a) P/n detector at zero bias, (b) Auger-suppressed detector in reverse bias.

level of doping, roughly a tenfold improvement over Rule 07 is predicted for Auger-suppressed detectors. The plot predicts that, if the doping can be further reduced to achieve the background radiation limit, dark current can be decreased to approximately 375 times below Rule 07 for 300 K operation. The method for achieving this limit is described in "Background Radiation-Limited Detector Performance".

BACKGROUND RADIATION-LIMITED DETECTOR PERFORMANCE

For the low levels of doping that Teledyne can regularly attain in HgCdTe, the easiest way to achieve very low carrier concentrations in the absorber region is to apply sufficient bias to fully deplete it, as shown in Fig. 5. By fully depleting the absorber, free carriers and Auger recombination are eliminated. If generation–recombination (G–R) currents are adequately low, the detector becomes limited by the background radiation.

Assuming a detector quantum efficiency η and background flux ϕ generated by the surrounding environment at temperature T, the detector current density, J^{Rad}, is, given by

$$J^{\mathrm{Rad}} = q\eta\phi(T), \tag{5}$$

which is simply the photo-generated current associated with the background radiation. Note that the detector quantum efficiency must be evaluated over all angles of incident radiation. Importantly, decreasing the background reduces the radiative currents. The fact that the photo-generated carriers are collected rather than allowed to recombine radiatively is the phenomenon known as negative luminescence.[8]

THE HETERO-JUNCTION P-I-N DETECTOR

Figure 6 shows an example of a P-ν-N detector that is compatible with background radiation-limited performance (BLIP). It makes use of Teledyne's DLPH P-on-n detector geometry and the low n-doping achievable with Teledyne's growth by MBE. The structure has a number of key features. The absorber layer is surrounded by a wider bandgap cap and buffer region in order to suppress dark current generation from these regions. The n-doping of the absorber is chosen to be sufficiently low to allow full depletion at moderate bias and the wide bandgap cap is used to suppress tunneling current under reverse bias; hence, the device is essentially a p-i-n diode. With a sufficiently wide bandgap cap,

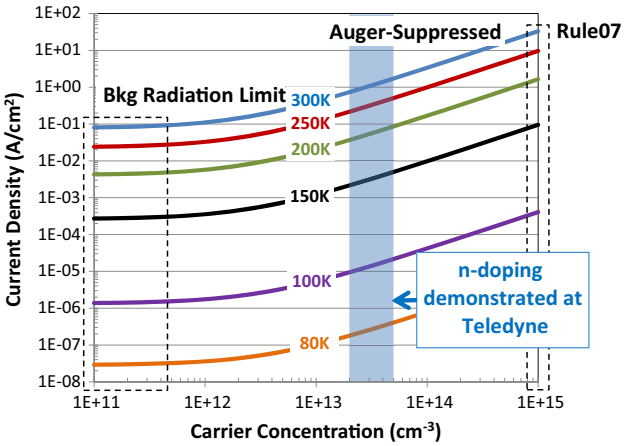

Fig. 4. Auger-suppressed dark current density for a 10-μm cutoff detector versus doping.

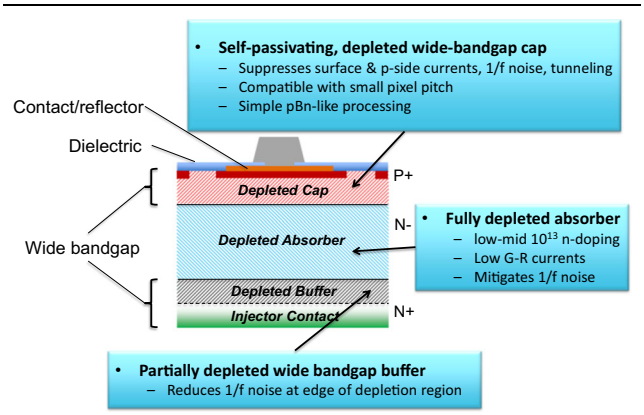

Fig. 6. Teledyne's hetero-junction p-i-n diode architecture.

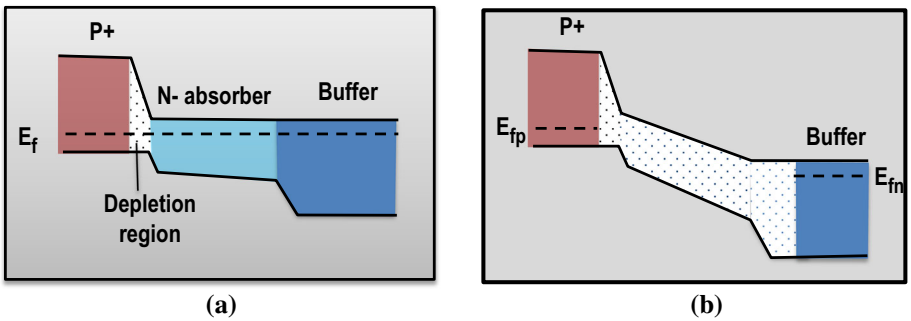

Fig. 5. Band diagram for a p-i-n diode (a) zero bias (b) reverse bias.

due to the planar nature of the architecture, the structure is potentially self-passivating, requiring only a few process steps for fabrication, and is analogous to the pBn geometry demonstrated in III–V detectors.[9] The fully-depleted geometry is also compatible with small pixel pitch, maintaining low crosstalk due to the built-in vertical electric field generated under detector reverse bias. As will be discussed in "Parasitic Effects", the fully depleted absorber and wide bandgap cap can potentially play a significant role in reducing $1/f$ and random telegraph noise.

Figure 7 shows the calculated dependence of absorber depletion width on detector bias and doping. For the range of doping achievable at Teledyne, a 5-μm-thick absorber can be fully depleted with between 0.1 V and 0.45 V reverse bias.

Figure 8 shows the calculated QE spectral response for a LWIR detector designed to a have a 10-μm cutoff when the absorber thickness is 10 μm. The quantum efficiency is observed to be quite reasonable within 1 μm of the detector cutoff for absorber thicknesses between 3 μm and 5 μm. Additional improvement to the QE near cutoff can be obtained by incorporating a reflective p-contact to generate a double-pass through the detector near cutoff.

In order for a fully depleted detector to have a current limited by background radiation, it is necessary that G–R currents in the depleted absorber be adequately low. The G–R current density, J_{GR}, is determined by the width of the depletion region, W_{dep}, and the Shockley–Read–Hall (SRH) lifetime, τ_{SRH}, and is given by the following expression

$$J_{GR} = q\frac{n_i}{\tau_{SRH}}W_{dep}. \quad (6)$$

Figure 9 compares the background radiation-limited current density with that for Rule 07 for 10-μm wavelength HgCdTe on an Arrhenius plot. Also shown are the G–R current components calculated for two different SRH lifetimes. The lifetimes are chosen to make G–R and background radiation currents equal at 300 K and 77 K, respectively. The data show that SRH lifetimes nominally greater than 30 μs and 15 ms are required to reach the background radiation limit at 300 K and 77 K, respectively.

Recently reported data on Teledyne LWIR detector arrays operating at 30 K for astronomy applications provide a very encouraging estimate for the achievable SRH lifetime.[10] Figure 10 shows an Arrhenius plot of representative pixel dark current in electrons/s/pixel for a 10.7-μm cutoff detector array having an 18-μm pixel pitch. The detectors were operated using a H1RG ROIC having a source-follower input circuit at a reverse bias of 240 mV. Dark current is observed to be diffusion-limited to

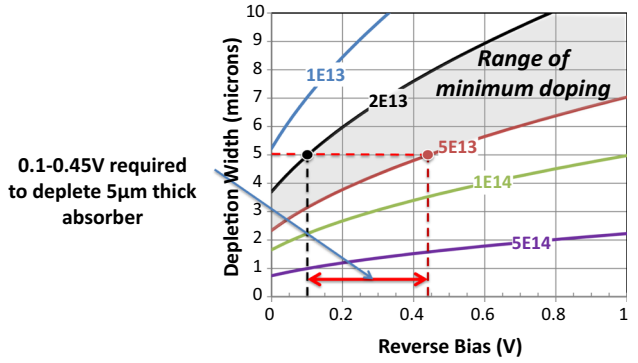

Fig. 7. Absorber depletion width versus reverse bias voltage and *n*-absorber doping.

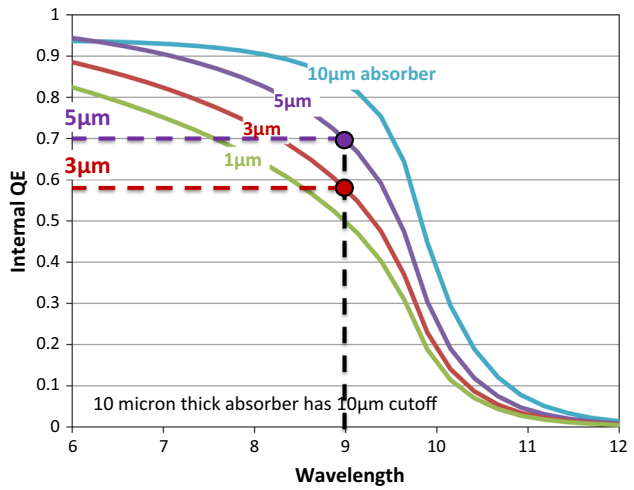

Fig. 8. Theoretical internal QE spectral response versus absorber layer thickness for a 10-μm cutoff detector.

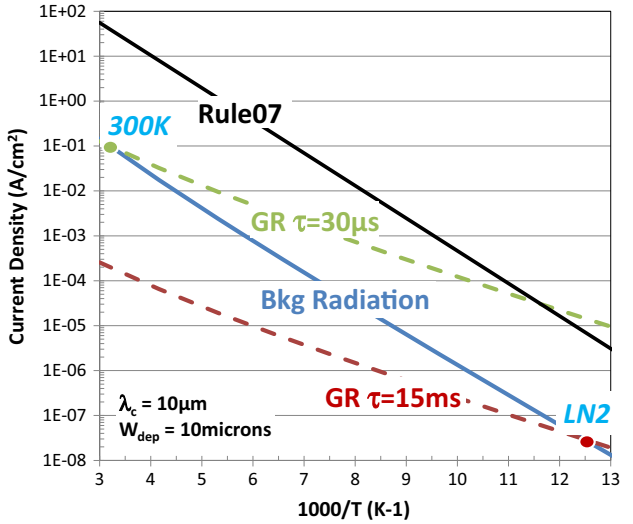

Fig. 9. Arrhenius plot of dark current density for radiatively-limited 10-μm cutoff HgCdTe compared to G–R current and Rule 07.

approximately 40 K and limited by light leakage in the dewar below this temperature. These data can be used to estimate an upper limit to the G–R current as shown by the dashed line in the figure. The fit was obtained using Eq. 6 with the usual assumption of a mid-gap trap and attributing all current above the diffusion-limited curve to G–R. It is important to note that the actual G–R current could be significantly lower. Using the detector depletion width associated with the detector at operating bias and the expression for G–R dark current given in Eq. 6, a lower limit to the SRH lifetime is estimated to be 100 ms.

To put this extracted lifetime into context, the computed values for Auger-suppressed dark current density versus temperature are shown for 10-μm cutoff HgCdTe in Fig. 11. The current density for three different absorber doping values is shown as well as the current density from background blackbody radiation integrated over pi steradians. Radiation current is observed to dominate for doping below approximately $1 \times 10^{13}/\text{cm}^3$. Also shown is the estimated G–R current based on the 100-ms SRH lifetime lower limit extracted from measurements of Teledyne's LWIR detectors at 30 K.

It is important to point out that the SRH lifetime extracted at 30 K is likely to be a minimum of 10 times lower at 300 K due to the increase in thermal velocity, which increases the probability of carrier capture by a recombination center. However, for the typical assumption that mid-gap traps are most efficient in the depletion region, the only other possibility for reduced lifetime is the shift of a trap energy level to within the bandgap as the gap widens with increasing temperature, which cannot be ruled out. Although the SRH lifetime at 30 K does not guarantee similar lifetimes at higher temperatures, it is at least very encouraging. However, as shown in Fig. 11, the 100-ms lower lifetime limit provides several orders of magnitude margin before reaching the level of thermal radiation from the environment.

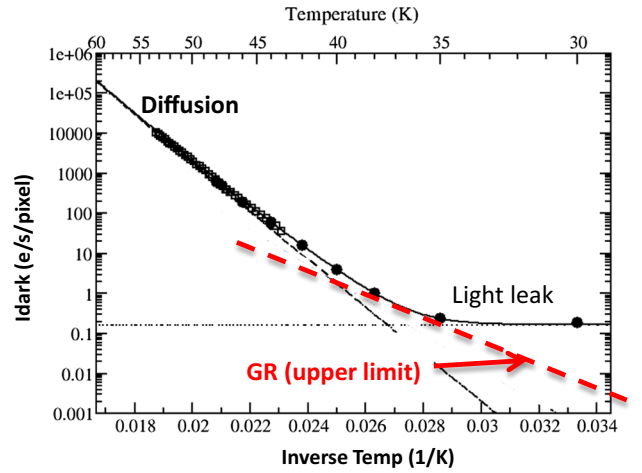

Fig. 10. Arrhenius plot of dark current for a 10.7-μm cutoff detector showing and estimated upper limit for G–R current.

PERFORMANCE BEYOND THE BACKGROUND RADIATION LIMIT

Because the background radiation-limited current is determined by thermal emission from the surrounding environment, it is potentially feasible to reduce this contribution to further lower the detector current. This can, in principle, be done without recourse to thermal cooling by use of negative-luminescence surfaces.[11–13]

To get a sense of the impact of various levels of current suppression from the background, Fig. 12 compares achievable background radiation-limited or background radiation-suppressed operating temperature to Rule 07 performance for short

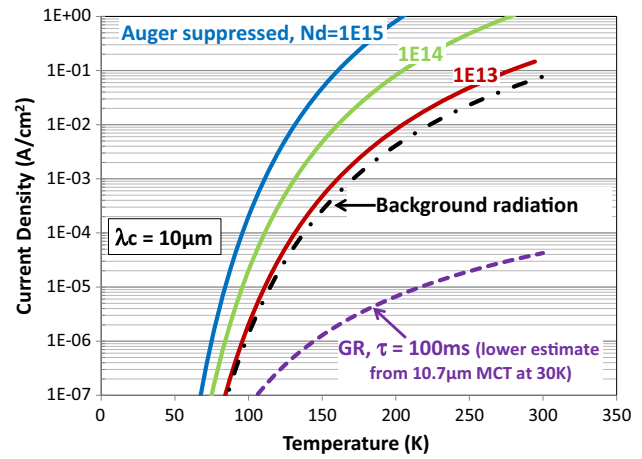

Fig. 11. Comparison of G–R current density extracted from 30-K lifetime measurements for Teledyne LWIR detectors with Auger-suppressed and background radiation current densities.

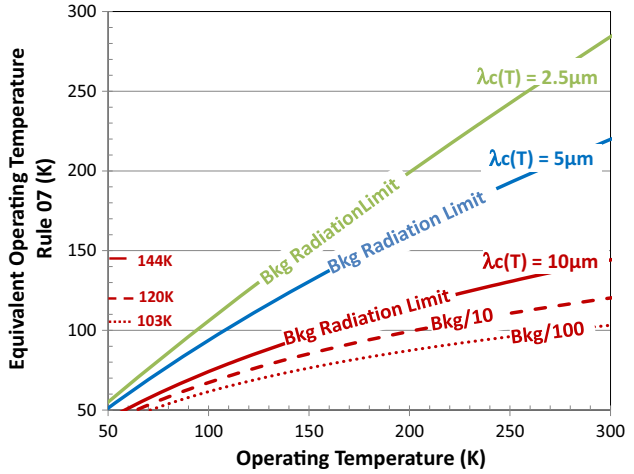

Fig. 12. Operating temperature for SWIR, MWIR and LWIR background radiation-limited detectors compared to conventional detectors obeying Rule 07.

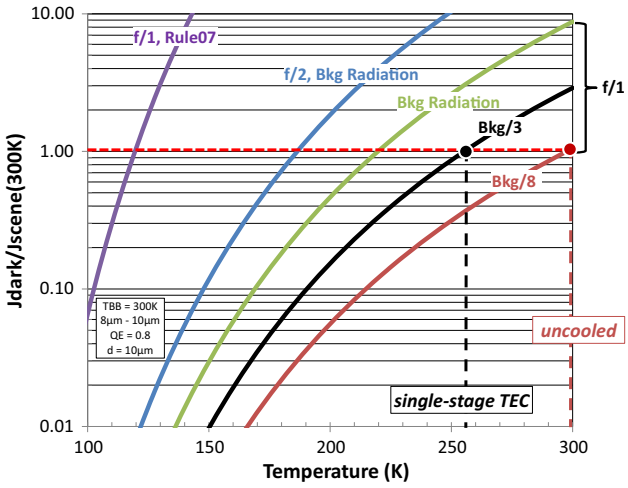

Fig. 13. Predicted operating temperature for background radiation-limited detectors using *f*/2 and *f*/1 optics.

wavelength infrared (SWIR), mid-wavelength infrared (MWIR) and LWIR.

For SWIR detectors, there is very little improvement in BLIP. For MWIR detectors, a maximum increase in operating temperature of approximately 80 K is obtained at 300 K over that of the same detector operating with Rule 07 performance. Obviously, if background radiation currents can be decreased using the techniques described above, larger increases in HOT performance can be achieved.

Examples of the impact of radiation current reduction are shown for LWIR detectors operating at 300 K. assuming 100%, 10%, and 1% backgrounds relative to blackbody radiation. The equivalent operating temperature for Rule 07 detectors are 144 K, 120 K and 103 K, respectively.

In the presence of illumination, the detector needs to have adequately low dark current to not significantly impact signal-to-noise. If 1/*f* noise is not present, then shot noise associated with the detector dark current can, in principal, be reduced relative to the signal by using sufficiently long integration times. In practice, the integration time is often limited by ROIC well capacity or system limitations on scene dwell time to prevent blurring.

As a conservative estimate, we can use the criteria that the detector does not generate more dark current than the signal photocurrent. This will increase the noise by $\sqrt{2}$. Figure 13 shows dark current density for 10-μm cutoff detectors as a function of temperature relative to scene photocurrent under *f*/2 and *f*/1 illumination. A detector quantum efficiency of 80% was assumed and three different radiation-background limits were evaluated. Also shown, for comparison, is the dark current for Rule 07.

The analysis indicates that single-stage TE-cooling can be used if the background radiation can be reduced to 1/3 of the blackbody radiation limit and 300 K operation is possible if the radiation contributions can be reduced to 1/8 of the blackbody radiation limit. Such an achievement could significantly change the landscape for HgCdTe for commercial and tactical applications due to the significant reduction in SWaP and cost associated with the Dewar and cooler assembly.

PARASITIC EFFECTS

There are a number of parasitic effects that can potentially limit the performance of the p-i-n heterojunction HgCdTe device. These include diffusion and G–R currents from both the *p*-side of the junction as well as from the neutral and depleted regions of the cap and buffer, defect-induced tunneling currents, spurious radiation from the Dewar, ROIC and cold finger, and 1/*f* noise or random telegraph noise (RTN). By appropriate design of the cap and buffer, it should be possible, in principle, to make the dark current contributions from these regions negligibly small. The impact from 1/*f* or random telegraph noise is perhaps less obvious.

Kinch[14] has argued that 1/*f* noise in HgCdTe detectors can result from modulation of diode diffusion and G–R dark current due to fluctuations in the size of depletion regions terminating on the detector surfaces. The size of the depletion region (and hence also the neutral region) is modulated by surface interface charge variations caused by trapping and de-trapping of carriers. The trapping phenomenon, which often has a 1/*f* noise spectral density, is well-known in the semiconductor industry and was first described by McWhorter[15] as being associated with a wide spectrum of trapping time constants that are usually found when carriers tunnel into and out of interfacial traps. The modulation effect explains the empirical linear relationship that is often used between 1/*f* noise and detector current. The coefficient of proportionality is often referred to as the Tobin coefficient.[16] In addition to modulation effects associated with the depletion region, similar types of modulation can result from fluctuations in surface recombination velocity driven by the same mechanism.[2,17] Due to the proportionality to dark current, 1/*f* noise is particularly problematic at high temperatures (HOT operation) where dark current is high. For the hetero-junction p-i-n structure, all depletion regions terminate in wide bandgap material. Thus, modulated noise currents associated with these regions will be exponentially reduced relative to the absorber, potentially resulting in a significant reduction in 1/*f* noise.

For an ideal detector, these mechanisms may be the only sources of 1/*f* noise. However, in practice, HgCdTe detectors are subject to threading dislocations associated with substrate defects. These dislocations are essentially un-passivated internal surfaces within the detector absorber region. Figure 14 shows diagrammatically the effect of such

a dislocation. The dislocation contains a core region with un-terminated bonds that distort the bands of the surrounding HgCdTe. In full analogy with the previous example, modulation of the charge in the core region can result in a corresponding modulation of the depletion region surrounding the dislocation and hence a fluctuation in the detector G–R and diffusion dark current and photocurrent.

Dislocations may also be a significant source of random telegraph noise (RTN). RTN currents in field effect transistor (FET) devices are well known and can be caused by single electron trapping and de-trapping at the oxide-channel interface, resulting in modulation of carrier density and mobility.[18] The time constants for the capture and emission typically exhibit an activation energy that determines the high-current and low-current dwell times. Similar channels may exist within dislocations, acting as conduction channels from the n-side of the junction to the p-side. For the example shown in Fig. 14, the p-side of the junction acts as the drain and the distributed source is supplied by carriers tunneling from the n-side of the absorber to the p-channel along a portion of the dislocation. However, for a fully depleted absorber, the probability for capture and emission of carriers from dislocations is expected to be very low due to the low density of available carriers and the rapid drift velocity of the carriers under the influence of the depletion region electric field. Thus, $1/f$ noise and RTN in these detectors may be fundamentally low.

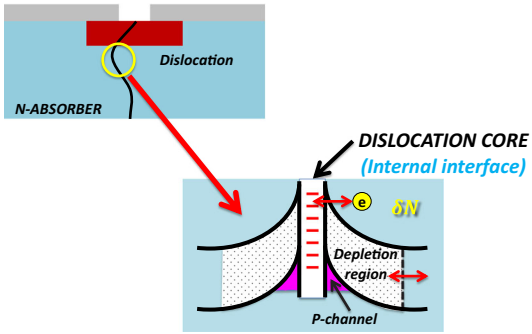

Fig. 14. Impact of dislocation on $1/f$ noise.

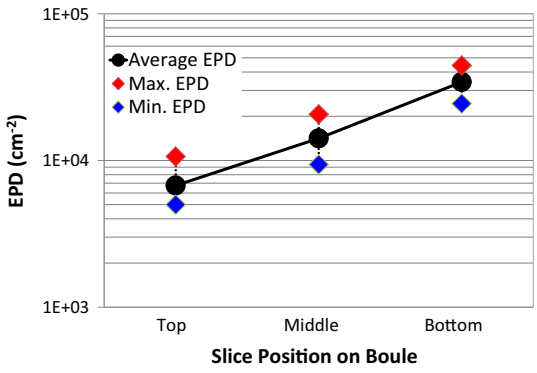

Fig. 15. Typical variation in EPD with slice position.

In addition to their impact on noise, dislocations can also be responsible for excess dark current, leading to decreased FPA operability. Often, trap-assisted tunneling current is observed for detectors when the junction intersects a dislocation for the reasons described. The probability of intersecting the dislocation is proportional to the density of dislocations as well as the detector junction area.

Dislocations in the CdZnTe substrate are the fundamental limitation to dislocations in the HgCdTe epi-layer. Typical etch pit densities, shown in Fig. 15, depend on the location of the slice position along the boule and range from the high, $10^3/cm^2$, to the middle, $10^4/cm^2$, ranges as measured using the Nakagawa defect etch.[19]

There are two approaches to improve the operability of detectors limited by dislocations: (1) improve the quality of the substrates and associated epitaxial layers, and (2) reduce the pixel size. The trend towards smaller pixel pitch has been ongoing for a number of years. It is motivated by a number of factors, including the trend to larger HD-format imagery, the drive to reduce costs by increasing the number of detector dies per wafer, improvements in processing and hybridization methods to allow for smaller pixels, and the realization that over-sampled pixel size provides certain system advantages.[20]

Figure 16 shows the calculated detector operability versus electrically-active defect density for 5-μm-sized LWIR pixels. Also shown is the estimated cumulative probability of achieving these defect densities. The probabilities are based on measured dislocation data from Teledyne and correlation between typical FPA operability and dislocation density for tactical applications. We estimate that approximately 10% of the dislocations are having an electrical impact on performance. As discussed, the

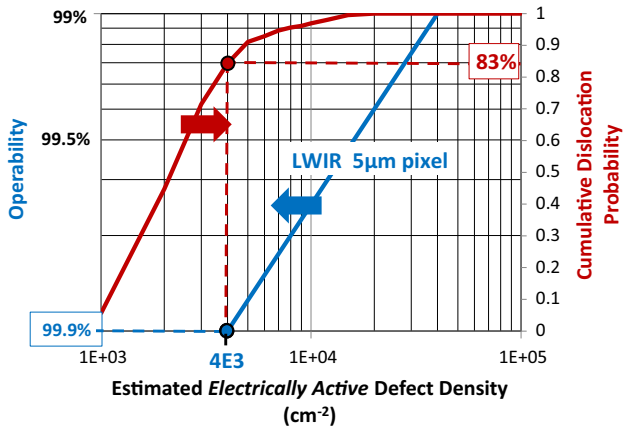

Fig. 16. Dependence of operability on electrically active defect density for 5-μm-pitch pixels compared with Teledyne-measured dislocation cumulative distribution, assuming 10% of dislocations are electrically active.

impact of dislocations may be particularly benign for the fully-depleted hetero-junction p-i-n architecture, so this estimate may be conservative. These results predict that 99.9% operability should be achieved for approximately 80% of the layers grown.

SUMMARY AND CONCLUSIONS

We have discussed how both absorber layer doping and Auger lifetime have equal footing in determining the dark current for Auger-limited detectors. It has been shown that suitably designed HgCdTe devices and structures can, in principle, operate with significantly lower dark current than is now typically achieved. These currents are made progressively lower first by Auger-suppression, then by Auger-elimination (the background radiation limit), and finally by suppressing the background radiation using special shielding techniques.

There are several key factors enabling such advances that have been demonstrated at Teledyne. These include

(1) The ability to *n*-type dope at the low to middle $10^{13}/cm^3$ range, permitting fully-depleted p-i-n devices to be operated at reasonable bias values and with good QE
(2) The demonstration of very long SRH lifetimes necessary to achieve background radiation-limited current or lower
(3) The ability to fabricate planar hetero-junction detectors with wide bandgap caps and buffers to reduce parasitic currents, $1/f$ and random telegraph noise.

If parasitic currents can be removed, modeling indicates that background radiation-limited LWIR HgCdTe operating with *f*/1 optics could operate within $\sqrt{2}$ of BLIP at 215 K. By reducing the background radiation by 2/3 using novel shielding methods, operation with a single-stage TE-cooler may be possible. If the background radiation can be reduced by 90%, then room-temperature operation is possible. These increases in operating temperature would provide a significant reduction in SWaP and costs for HgCdTe IDCAs and cameras for many applications.

The drive towards small pixels also affords another advantage to the hetero-junction PIN diode structure. Since it is fully depleted and planar, it is compatible with a small pixel pitch while maintaining low crosstalk and simple processing akin to pBn structures.

By combining smaller pixels, simpler processing, reduced Dewar and cooler requirements with the continual increase in size and lower dislocation densities of CdZnTe substrates, future HgCdTe detectors may offer both a cost and performance advantage over other technologies for many years to come.

REFERENCES

1. C.H. Grein, P.M. Young, and H. Ehrenreich, *Appl. Phys. Lett.* 61, 2905 (1992).
2. M. Kinch, *Fundamentals of Infrared Detector Materials* (Bellingham: SPIE, 2007), p. 33.
3. T. Ashley and C.T. Elliot, *Electron. Lett.* 21, 451 (1985).
4. T. Ashley, C.T. Elliot, and A.T. Harker, *Infrared Phys.* 26, 303 (1986).
5. P. Martyniuk and A. Rogalski, *Opto Elect. Rev.* 21, 240 (2013).
6. W. Tennant, D. Lee, M. Zandian, E. Piquette, and M. Carmody, *J. Electron. Mater.* 37, 1406 (2008).
7. W.E. Tennant, *J. Electron. Mater.* 39, 1030 (2010).
8. T. Ashley, N. Gordon, G. Nash, C. Jones, C. Maxey, and R. Catchpole, *Appl. Phys. Lett.* 79, 1136 (2001).
9. P. Klipstein, D. Aronov, E. Berkowicz, R. Fraenkel, A. Glozman, S. Grossman, O. Klin, I. Lukomsky, I. Shtrichman, N. Snapi, M. Yassem, and E. Weiss, *SPIE Newsroom* (2011). doi:10.1117/2.1201111.003919.
10. C. McMurtry, D. Lee, J. Beletic, A. Chen, R. Demers, M. Dorn, D. Edwall, C.B. Fazar, W. Forrest, F. Liu, A. Mainzer, J. Pipher, and A. Yulius, *Opt. Eng.* 52, 091804 (2014).
11. J. Lindle, W. Bewley, I. Vurgaftman, C.S. Kim, J. Meyher, J. Johnson, M. Thomas, E. Piquette, and W. Tennant, *IEEE J. Quant. Electron.* 41, 227 (2005).
12. P. Capper and C.T. Elliot, *Infrared Detectors and Emitters: Materials and Devices* (New York: Springer, 2001), p. 197.
13. W. Tennant, U.S. patent 20070290132.
14. M. Kinch, *Appl. Phys. Lett.* 94, 193508 (2007).
15. A.L. McWhorter, *Semiconductor Surface Physics* (Philadelphia: University of Pennsylvania Press, 1957), p. 207.
16. S. Tobin, *IEEE Trans. Electron. Devices* 27, 43 (1980).
17. D. Lee, S. Liberman, and A. Mestechkin, *Proc. IRIS Detect.* 1, 109 (1992).
18. M.H. Tsai, T.P. Ma, and T.B. Hook, *IEEE Electron. Device Lett.* 15, 504 (1994).
19. R. Hirano, JX Materials, unpublished research, 2015.
20. J. Caulfield, J. Curzan, J. Lewis, N. Dhar, in *Proc. SPIE*, (2015), p. 9451.